

Nonlinear Quantum Behavior of Ultrashort-Pulse Optical Parametric Oscillators

Tatsuhiko Onodera,^{1,*} Edwin Ng,^{1,*} Niels Lörch,^{1,2} Atsushi Yamamura,¹
Ryan Hamerly,³ Peter L. McMahon,^{1,4,5} Alireza Marandi,⁶ and Hideo Mabuchi^{1,†}

¹*E. L. Ginzton Laboratory, Stanford University, Stanford, CA 94305, USA*

²*Department of Physics, University of Basel, Klingelbergstrasse 82, 4056 Basel, Switzerland*

³*Research Laboratory of Electronics, Massachusetts Institute of Technology, Cambridge, MA 02139, USA*

⁴*National Institute of Informatics, 2-1-2 Hitotsubashi, Chiyoda-ku, Tokyo 101-8430, Japan*

⁵*School of Applied and Engineering Physics, Cornell University, Ithaca, NY 14853, USA*

⁶*California Institute of Technology, Pasadena, CA 91125, USA*

(Dated: February 13, 2019)

The quantum features of ultrashort-pulse optical parametric oscillators (OPOs) are theoretically investigated in the nonlinear regime near and above threshold. Starting from basic premises of input-output theory, we derive a general quantum model for pulsed OPOs subject to $\chi^{(2)}$ interactions between a multimode signal cavity and a non-resonant broadband pump field, elucidating time scale conditions required for such pulsed OPOs to admit an input-output description. By employing a supermode decomposition of the nonlinear Lindblad operators governing pump-signal interactions, we perform multimode quantum simulations in the regime of strong nonlinearity and study effects such as pump depletion and corrections to the squeezing spectrum of the linearized model. We observe non-Gaussian states with Wigner function negativity and show that multimode interactions with the pump can act as decoherence channels.

I. INTRODUCTION

Ultrashort-pulse OPOs have become established as an ideal testbed for the generation and manipulation of coherent nonlinear interactions among many optical frequency modes at once. In the classical domain, pulsed OPOs are used to generate frequency combs for applications in molecular spectroscopy and atomic clocks [1–4], and the strong temporal confinement of the field facilitates efficient nonlinear optics [5]. In quantum experiments, they have been synchronously pumped below threshold to generate multimode squeezed light [6–8]. Because their quantum states intrinsically reside in a multimode Hilbert space of high dimensionality, they are also being investigated as a resource for optical quantum information processing [9–12].

Many of the quantum features of pulsed OPOs are inherited from their single-mode continuous-wave (cw) counterparts, including squeezing [13], non-Gaussian state generation [14], and their applications to quantum information and communication [15, 16]. Quantum input-output theory [17, 18] has been pivotal in elucidating the properties of cw OPOs, as the formalism makes numerical simulation (e.g., via the Lindblad master equation or quantum trajectories) tractable by reducing the interactions among optical fields in the OPO to the dynamics of a single internal mode interacting with a white-noise reservoir [19, 20]. The result is that a wide range of sophisticated techniques, from quantum measurement and feedback to quantum coherent control [21, 22], have been applied to the analysis of cw OPO dynamics and networks [23, 24].

Looking towards the goal of performing quantum and coherent information processing in optical systems, an especially intriguing feature of OPOs is the onset of nonlinear dynamics near and above threshold, which can be exploited to perform useful computational tasks [25–29]. When such nonlinearities occur in the quantum regime, cw OPOs have been theoretically shown to generate non-Gaussian states [14], which form the basis for schemes in quantum computation [30, 31] and quantum-enhanced metrology [31, 32].

In this context, it is interesting to ask whether quantum input-output theory can be applied to pulsed OPOs in the above-threshold regime. At first glance, input-output theory seems ill-suited as there is a large number of internal cavity modes (typically 10^4 to 10^5). However, in Refs. [33, 34], it was shown that despite the daunting number of modes, it is possible to construct an input-output theory for synchronously-pumped OPOs resonating many signal frequencies at once. In their work, the authors derived multimode Heisenberg equations of motion for the interactions between a free-field pump and the signal modes of the OPO, and they linearized those equations in the below-threshold, weakly-nonlinear regime. The key observation was the resulting input-output model can be simplified by moving to a supermode basis [12, 35] for the resonant cavity modes.

In this work we extend the technique of Refs. [33, 34] to obtain supermode descriptions of the *nonlinear* interactions as well, in order to study the near- and above-threshold behavior of pulsed OPOs interacting with a free-field pump. With an eye towards Schrödinger-picture numerical simulations via the Lindblad master equation or quantum trajectories [18], we cast the input-output theory in Lindblad form, with an emphasis on the nonlinear Lindblad operators that dominate the OPO physics near and above threshold. In the process, we de-

* These authors contributed equally to this work.

† hmabuchi@stanford.edu

fine “band-limited” quantum noise operators which reduce to the noise operators in Ref. [34] under appropriate timescale limits, thus clarifying the assumptions required for an input-output model—formulated in continuous time by construction—to be compatible with the pulsed nature of the system. Using the input-output formalism, we show by numerical simulation a variety of nonlinear effects in the model, such as pump depletion, corrections to the linearized squeezing spectrum, and the generation of non-Gaussian states.

The paper is structured as follows. In Sect. II, we derive the input-output theory of pulsed OPOs and find conditions under which the white-noise assumption of input-output theory holds. In Sect. III, we specialize the theory to the case of quasi-degenerate, synchronously-pumped OPOs. We review the physical implications of phase-matching in Sect. IV and the supermode formalism, including its application to the nonlinear Lindblad operators, in Sect. V. Finally in Sect. VI, we discuss the phenomenology of the nonlinear theory, including: a discussion on the white-noise approximation, a derivation of the nonlinear Heisenberg equations of motion in the supermode basis, and the results of our numerical simulations exhibiting nonlinear and multimode phenomena in synchronously-pumped OPOs.

II. MULTIMODE INPUT-OUTPUT THEORY OF PULSED OPOS

The input-output formalism deals with systems coupled weakly to a reservoir, which we take to be a good characterization of a high-finesse pulsed OPO (the system) coupled to free propagating optical fields (the reservoir) [17, 18]. The systems we consider consist of a broadband set of resonant modes in a “signal” band of frequencies and are schematically shown in Fig. 1. The system exhibits linear coupling to a corresponding signal band \mathcal{S} in the free field and *nonlinear* coupling to a second-harmonic “pump” band \mathcal{P} , also in the free field. Following the usual procedure for high-finesse optical systems, we assume the system (quasi-)modes can be quantized independently of the reservoir, and we derive perturbatively the system dynamics subject to the effects of the reservoir in an input-output framework.

Let the cavity resonate a set of signal modes, with resonance frequencies ω_{sm} . We suppose the resonant signal modes are described by an electric displacement field operator $\hat{\mathbf{D}}_s(\mathbf{r}, t)$ of the form

$$\hat{\mathbf{D}}_s(\mathbf{r}, t) = i \sum_m \mathbf{D}_{sm}(\mathbf{r}) \hat{s}_m e^{-i\omega_{sm}t} + \text{H.c.} \quad (1)$$

in the interaction frame of the linear Hamiltonian, where $[\hat{s}_m, \hat{s}_n^\dagger] = \delta_{mn}$ and $\mathbf{D}_{sm}(\mathbf{r})$ are appropriately chosen mode functions, as prescribed by canonical quantization of the macroscopic Maxwell’s equations [36, 37].

It is worth noting that in the derivation to follow, we do not necessarily assume uniform cavity mode spacing,

which is the case depicted in Fig. 1(c). One example of this special case is addressed in more detail in Sect. III. In general, however, cavity resonances may not be uniformly spaced, either due to intracavity dispersion (especially in broadband cavities) or because the system may consist of multiple coupled cavities, as depicted in Fig. 1(b), resulting in the “resonance splitting” in Fig. 1(d). The following derivation can be applied to these nonuniform cases as well.

A. Linear dissipation

We begin by treating the linear coupling to the reservoir at the signal frequency band. Aside from outcoupling, this can also describe linear losses due to scattering or other intrinsic imperfections; while such effects are by nature spatially multimode, we take the usual assumption that, for each cavity mode, the various scattering channels can be combined into a single effective coupling to the reservoir, following Wigner-Weisskopf [38].

We introduce reservoir modes \hat{b}_ω , with $[\hat{b}_\omega, \hat{b}_{\omega'}^\dagger] = 2\pi\delta(\omega - \omega')$ in a signal frequency range \mathcal{S} of interest, and posit a minimal-coupling Hamiltonian in the interaction frame of the form

$$\hat{V}_{\text{lin}} := i \sum_m \int_{\mathcal{S}} \frac{d\omega}{2\pi} \sqrt{2\kappa_m} \hat{s}_m \hat{b}_\omega^\dagger e^{-i(\omega_{sm} - \omega)t} + \text{H.c.}, \quad (2)$$

where we have made the Markov assumption that the coupling coefficients κ_m are constant around ω_{sm} ; in this case, κ_m is the field decay rate for the m th signal mode.

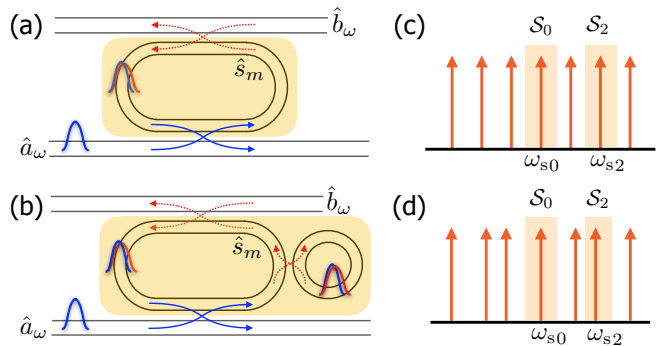


FIG. 1. Schematic of various systems of pulsed OPOs and their resulting cavity mode structure. In (a), a single resonator (highlighted in yellow) is coupled on the bottom to a propagating pump field through a dichroic and on top to a propagating signal field through an outcoupler, resulting in (c) a set of uniformly spaced resonances. In (b), two coupled resonators form a single system (highlighted in yellow), resulting in (d) a nonuniform mode structure. In both cases, only the signal is resonant in the system, and the cavity medium (i.e., region in yellow) is taken to contain the $\chi^{(2)}$ nonlinearity (with appropriate dispersion compensation). The highlights in (c,d) indicate the bands \mathcal{S}_m over which we define signal input-output operators (see main text).

To further develop this interaction, we define a set of “band-limited” reservoir operators

$$\hat{b}_t^{(m)} := \int_{\mathcal{S}_m} \frac{d\omega}{2\pi} \hat{b}_\omega e^{-i(\omega - \omega_{s_m})t}, \quad \text{where} \quad (3)$$

$$\mathcal{S}_m := \left(\frac{1}{2}(\omega_{s_m} + \omega_{s_{m-1}}), \frac{1}{2}(\omega_{s_m} + \omega_{s_{m+1}}) \right), \quad (4)$$

as illustrated in Fig. 1(c). The commutation relations for these band-limited operators have an interesting structure. Defining $\Delta\omega_{s_m}^{(-)} := \frac{1}{2}(\omega_{s_m} - \omega_{s_{m-1}})$ and $\Delta\omega_{s_m}^{(+)} := \frac{1}{2}(\omega_{s_{m+1}} - \omega_{s_m})$,

$$[\hat{b}_t^{(m)}, \hat{b}_{t'}^{(m')\dagger}] = \delta_{mm'} \int_{-\Delta\omega_{s_m}^{(-)}}^{+\Delta\omega_{s_m}^{(+)}} \frac{d\omega}{2\pi} e^{-i\omega(t-t')} \quad (5)$$

$$\rightarrow \delta_{mm'} \delta(t-t') \quad \text{as} \quad \Delta\omega_{s_m}^{(\pm)} \rightarrow \infty. \quad (6)$$

The latter white-noise approximation to the commutator holds whenever the signal mode spacings $\Delta\omega_{s_m}^{(\pm)}$ dominate all other coupling rates in the system. Using these new modes as the reservoir degrees of freedom, we can rewrite the minimal-coupling Hamiltonian as

$$\hat{V}_{\text{lin}} = i \sum_m \hat{b}_t^{(m)\dagger} \sum_n \sqrt{2\kappa_n} \hat{s}_n e^{-i(\omega_{s_n} - \omega_{s_m})t} + \text{H.c.} \quad (7)$$

In the white-noise limit of (6), the Hamiltonian (7) formally defines a quantum input-output model with linear Lindblad operators

$$\hat{L}_{\text{lin}}^{(m)} := \sum_n \sqrt{2\kappa_n} e^{-i(\omega_{s_n} - \omega_{s_m})t} \hat{s}_n \approx \sqrt{2\kappa_m} \hat{s}_m, \quad (8)$$

and the system dynamics are described by the corresponding Lindblad master equation. Note that the conditions under which the last rotating wave approximation in (8) holds coincide with the validity of the input-output interpretation itself: both are valid provided the white-noise limit $\Delta\omega_{s_m}^{(\pm)} \rightarrow \infty$ holds.

B. Nonlinear parametric interactions

We now turn to the treatment of the nonlinear $\chi^{(2)}$ interaction between the cavity signal modes and the non-resonant pump field. We suppose the pump is described as a spectrally continuous field, with an electric displacement field operator $\hat{\mathbf{D}}_p$ of the form

$$\hat{\mathbf{D}}_p(\mathbf{r}, t) = i \int_{\mathcal{P}} \frac{d\omega}{2\pi} \mathbf{D}_{p\omega}(\mathbf{r}) \hat{a}_\omega e^{-i\omega t} + \text{H.c.} \quad (9)$$

in the interaction frame of the linear Hamiltonian, where the continuum pump reservoir modes \hat{a}_ω obey $[\hat{a}_\omega, \hat{a}_{\omega'}^\dagger] = 2\pi\delta(\omega - \omega')$ and $\mathbf{D}_{p\omega}(\mathbf{r})$ are appropriately chosen continuum mode profile functions, as prescribed by canonical quantization of the macroscopic Maxwell’s equations [36, 37]. The frequency range \mathcal{P} for this integral (i.e., the pump band) should be sufficiently confined so as to not overlap with the signal reservoir band \mathcal{S} .

We take the macroscopic nonlinear $\chi^{(2)}$ Hamiltonian in the interaction frame to be [36, 37]

$$\begin{aligned} \hat{V}_{\text{nl}} &:= \int d^3\mathbf{r} \sum_{i,j,k} \eta_{ijk}^{(2)}(\mathbf{r}) \hat{D}_p^i(\mathbf{r}) \hat{D}_s^j(\mathbf{r}) \hat{D}_s^k(\mathbf{r}) \\ &= i \int \frac{d\omega}{2\pi} \hat{a}_\omega^\dagger \sum_{m,n} f_{mn}(\omega) \hat{s}_m \hat{s}_n e^{-i(\omega_{s_m} + \omega_{s_n} - \omega)t} + \text{H.c.}, \end{aligned} \quad (10)$$

where $\eta_{ijk}^{(2)}(\mathbf{r})$ is the second-order inverse susceptibility tensor [36] (assumed to be frequency independent), and the coupling strength of the three-wave interaction is

$$f_{mn}(\omega) := \int d^3\mathbf{r} \sum_{i,j,k} \eta_{ijk}^{(2)}(\mathbf{r}) (D_{p\omega}^{i*} D_{s_m}^j D_{s_n}^k)(\mathbf{r}). \quad (11)$$

We can follow a similar procedure as in the linear dissipation case in order to derive input-output pump operators. The choice of partitions \mathcal{P}_q of the pump frequencies is somewhat arbitrary; if the pump is a frequency comb, for example, one natural choice is to use the pump comb lines. In any case, let us denote such pump frequencies of interest as ω_{p_q} . We now define pump operators

$$\hat{a}_t^{(q)} := \int_{\mathcal{P}_q} \frac{d\omega}{2\pi} \hat{a}_\omega e^{-i(\omega - \omega_{p_q})t}, \quad \text{where} \quad (12)$$

$$\mathcal{P}_q := \left(\frac{1}{2}(\omega_{p_q} + \omega_{p_{q-1}}), \frac{1}{2}(\omega_{p_q} + \omega_{p_{q+1}}) \right). \quad (13)$$

Defining $\Delta\omega_{p_q}^{(+)} := \frac{1}{2}(\omega_{p_q} - \omega_{p_{q-1}})$ and $\Delta\omega_{p_q}^{(-)} := \frac{1}{2}(\omega_{p_{q+1}} - \omega_{p_q})$, the commutators are

$$[\hat{a}_t^{(q)}, \hat{a}_{t'}^{(q')\dagger}] = \delta_{qq'} \int_{-\Delta\omega_{p_q}^{(-)}}^{+\Delta\omega_{p_q}^{(+)}} \frac{d\omega}{2\pi} e^{-i\omega(t-t')} \quad (14)$$

$$\rightarrow \delta_{qq'} \delta(t-t') \quad \text{as} \quad \Delta\omega_{p_q}^{(\pm)} \rightarrow \infty. \quad (15)$$

Once again, the pump operators obey a white-noise limit when the pump frequency spacings $\Delta\omega_{p_q}^{(\pm)}$ are large compared to all other coupling rates in the system.

Finally, we make the Markov assumption that the coupling strengths f_{mn} are independent of the pump frequencies within each partition \mathcal{P}_q . That is, $f_{mn}^{(q)} := f_{mn}(\omega_{p_q}) \approx f_{mn}(\omega)$ for any $\omega \in \mathcal{P}_q$. With this assumption, the nonlinear Hamiltonian in terms of the pump operators becomes

$$\hat{V}_{\text{nl}} = i \sum_q \hat{a}_t^{(q)\dagger} \sum_{m,n} f_{mn}^{(q)} \hat{s}_m \hat{s}_n e^{-i(\omega_{s_m} + \omega_{s_n} - \omega_{p_q})t} + \text{H.c.} \quad (16)$$

In the white-noise limit of (15), the Hamiltonian (16) formally defines a quantum input-output model with nonlinear Lindblad operators

$$\hat{L}_{\text{nl}}^{(q)} := \sum_{m,n} f_{mn}^{(q)} \hat{s}_m \hat{s}_n e^{-i(\omega_{s_m} + \omega_{s_n} - \omega_{p_q})t}. \quad (17)$$

Note that in general, if the pump frequencies ω_{p_q} are arbitrarily picked relative to the signal frequencies ω_{s_m} , one may not be able to apply a rotating wave approximation to simplify these Lindblad operators further.

C. System Hamiltonian under pumping

Up to this point, we have not yet specified a *system* Hamiltonian, as (7) and (16) only describe the interaction between the signal modes and the environment. However, if we now introduce coherent drives at the pump frequencies, we displace the nonlinear Lindblad operators by

$$\hat{L}_{\text{nl}}^{(q)} \mapsto \hat{L}_{\text{nl}}^{(q)} + \alpha^{(q)} \quad (18)$$

and produce a multimode squeezing Hamiltonian

$$\hat{H}_{\text{sys}} = \frac{i}{2} \sum_q \alpha^{(q)*} \sum_{m,n} f_{mn}^{(q)} \hat{s}_m \hat{s}_n e^{-i(\omega_{sm} + \omega_{sn} - \omega_{pq})t} + \text{H.c.} \quad (19)$$

This Hamiltonian is the broadband version of the usual quadratic Hamiltonian for an cw OPO below threshold and is in agreement with prior derivations through other means, such as by assuming a resonant but adiabatically-eliminated multimode pump [34].

This model, however, is not limited only to pump driving. As a benefit of having a full quantum input-output model, (8) and (17) allow us to construct a wide variety of system Hamiltonians and Lindblad operators via dissipation engineering, e.g., in an SLH formalism [21].

III. THE QUASI-DEGENERATE SYNCHRONOUSLY-PUMPED OPO

A very important special case of the above theory applies to the quasi-degenerate synchronously-pumped OPO (SPOPO), in which

- the system consists of a cavity resonating a uniform comb of signal modes with free spectral range Ω (i.e., any mode dispersion due to the nonlinear medium is compensated elsewhere in the cavity), as illustrated in Fig. 1(c);
- the system is pumped by a classical frequency comb (e.g., as produced by a mode-locked laser), with comb spacing (i.e., pulse repetition rate) equal to Ω (*synchronous pumping*);
- the phase matching is chosen such that maximal nonlinear coupling strength occurs between the center signal mode at frequency ω_0 and the center pump line at frequency $2\omega_0$, but there is still sufficient phase matching off-center to facilitate non-degenerate interactions within the system optical bandwidth (*quasi-degenerate*).

For such a system, it is convenient to enumerate the cavity signal modes as $\omega_{sm} = \omega_0 + m\Omega$ and the pump frequencies as $\omega_{pq} = 2\omega_0 + q\Omega$.

We now assume, on top of the Markov assumptions, that the system satisfies the white-noise assumptions of Sect. II, for both the signal and pump reservoir modes.

These assumptions enable a rotating wave approximation on the nonlinear Lindblad operators to allow only energy-conserving interactions, such that the only contributions to the sum in (17) obey $m + n = q$. That is, the multimode Lindblad operators for an input-output theory of such SPOPOs can be reduced to

$$\hat{L}_{\text{lin}}^{(m)} = \sqrt{2\kappa_m} \hat{s}_m \quad (20a)$$

$$\hat{L}_{\text{nl}}^{(q)} = \sum_{m+n=q} f_{mn}^{(q)} \hat{s}_m \hat{s}_n. \quad (20b)$$

Finally, to arrive at the synchronously-pumped aspect of this model, we take the pump amplitude at frequency ω_{pq} to have amplitude α_q . Here, we arrive at the SPOPO version of (19), where we displace

$$\hat{L}_{\text{nl}}^{(q)} \mapsto \hat{L}_{\text{nl}}^{(q)} + \alpha^{(q)}, \quad (21)$$

and pick up the SPOPO system Hamiltonian

$$\hat{H}_{\text{sys}} = \frac{i}{2} \sum_{m+n=q} \alpha^{(q)*} f_{mn}^{(q)} \hat{s}_m \hat{s}_n + \text{H.c.} \quad (22)$$

Equations (20) through (22) provide a full quantum input-output model for quasi-degenerate SPOPO.

IV. PHASE MATCHING

It is clear that the coupling coefficients $f_{mn}^{(q)}$ play a crucial role in the physics of this model, as they affect both the nonlinear Lindblad operators as well as the system Hamiltonian under pump drive. The physical considerations that govern the structure of $f_{mn}^{(q)}$ are determined through the three-wave interaction integral (11), which in turn is dictated by the cavity mode profiles and the phase matching of the $\chi^{(2)}$ interactions.

To get intuition for the typical structure of $f_{mn}^{(q)}$, we can consider some physical assumptions for both the cavity modes and the phase-matching conditions. We assume the signal modes, pump frequencies, and cavity dispersion are set consistently with the SPOPO model introduced in Sect. III. Then the coupling coefficients can be summarized using a symmetric matrix $F_{mn} := f_{mn}^{(m+n)}$. The coefficients of the nonlinear Lindblad operator $\hat{L}_{\text{nl}}^{(q)}$ in (20b) form the q th diagonal of F_{mn} .

Let us also consider the special case of a one-dimensional cavity containing a section of nonlinear $\chi^{(2)}$ material, and that the pump and signal modes propagate along the cavity optical axis z with a one-dimensional phase front (i.e., are mostly collimated) in the region where there is material nonlinearity. Then the mode functions can be written as

$$\mathbf{D}_{sm}(\mathbf{r}) = \mathbf{D}_{sm}(\mathbf{r}_\perp) e^{ik_z(\omega_{sm})z} \quad (23a)$$

$$\mathbf{D}_{pq}(\mathbf{r}) = \mathbf{D}_{pq}(\mathbf{r}_\perp) e^{ik_z(\omega_{pq})z}, \quad (23b)$$

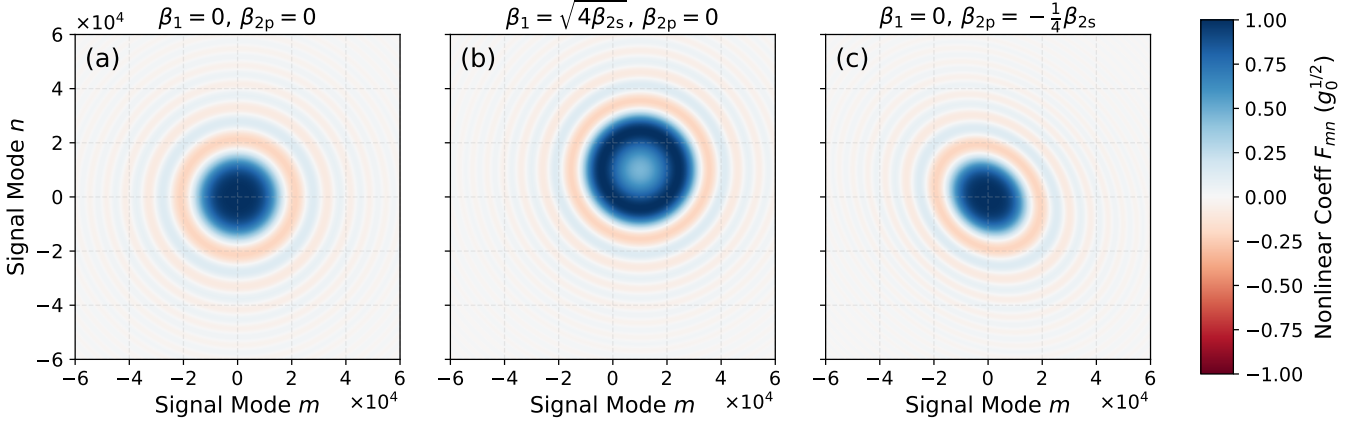


FIG. 2. Structure of the nonlinear coupling coefficients $F_{mn}/\sqrt{g_0} = \text{sinc}(\Phi_{mn})$, assuming an SPOPO with $g_{mn} \approx g_0$, for various material dispersion parameters chosen according to the second-order expansion (28). In all three cases shown here, β_{2s} limits the phase-matching bandwidth, and we fix $\beta_{2s} = 10^{-8}$ to correspond to $\sim 10^4$ phase-matched comb lines for tens-of-femtosecond pulses with GHz repetition rates.

where $k_z(\omega)$ is the z -component of the wavevector and \mathbf{r}_\perp is transverse to z . We also take the material nonlinearity to have a one-dimensional modulation due to quasi-phase-matching with period k_{qpm} [39]:

$$\eta_{ijk}^{(2)}(\mathbf{r}) = \eta_{ijk}^{(2)}(\mathbf{r}_\perp) \sin(k_{\text{qpm}}z) \quad (24)$$

Inserting these relations into (11), the matrix we are interested in can be written as [40]

$$F_{mn} \approx g_{mn}^{1/2} \text{sinc}(\Phi_{mn}), \quad (25)$$

assuming $k_z(2\omega_0) - k_z(\omega_0) \gg 1/L$, with coupling rates g_{mn} and phase mismatch functions Φ_{mn} given by

$$g_{mn}^{1/2} := \frac{L}{2} \int d^2\mathbf{r}_\perp \eta_{ijk}^{(2)}(\mathbf{r}_\perp) (D_{\text{pm}+n}^{i*} D_{\text{sm}}^j D_{\text{sn}}^k)(\mathbf{r}_\perp) \quad (26)$$

$$\Phi_{mn} := \frac{k_{\text{qpm}} + k_z(\omega_{sm}) + k_z(\omega_{sn}) - k_z(\omega_{\text{pm}+n})}{2/L}. \quad (27)$$

In the following discussion, we make the further assumption that g_{mn} is approximately constant across the wavelengths of interest and we denote its value by g_0 .

Finally, we can posit a form for the phase mismatch. By the quasi-degenerate nature of the SPOPO, we have $k_z(2\omega_0) - 2k_z(\omega_0) = k_{\text{qpm}}$, or that $\Phi_{00} = 0$. Then, if the dispersion is sufficiently smooth within the wavelengths of interest, we can expand (27) to second order as

$$\Phi_{mn} \approx \beta_1(m+n) + \beta_{2p}(m+n)^2 - \beta_{2s}(m^2+n^2), \quad (28)$$

where $\beta_1 := \frac{1}{2}\Omega(\text{GVM})L$, $\beta_{2s} := \frac{1}{4}\Omega^2(\text{GDD}_p)$, and $\beta_{2p} := \frac{1}{4}\Omega^2(\text{GDD}_s)$. Here, the material dispersion parameters are GVM, the group velocity mismatch of pump relative to signal and GDD_p (GDD_s), the group delay dispersion of pump (signal), both evaluated at ω_0 for signal and $2\omega_0$ for pump. Fig. 2 shows some typical forms for $\text{sinc}(\Phi_{mn})$ under this expansion.

It is worth noting that an approximation like (28) implicitly makes a few additional assumptions. In the absence of signal dispersion ($\beta_{2s} = 0$), there is perfect phase matching for all opposite frequency pairs $m = -n$. Similarly, when $\beta_{2p} > \frac{1}{2}\beta_{2s}$, the perfect phase matching occurs along hyperbolic sections. In these cases, a second-order expansion is inappropriate, as third-or-higher-order dispersion (or pump bandwidth) would then be responsible for limiting the interactions in a realistic system.

V. CONSTRUCTION OF SUPERMODES

Given the possibly large number of Lindblad operators and internal cavity modes, it is natural to ask whether there is a more efficient basis in which to describe the interactions than via individual frequency modes. In general, one can apply any arbitrary basis transformation on the continuum pump modes to obtain new pump “supermode” operators

$$\hat{A}_t^{(k)} := \sum_q R_{kq} \hat{a}_t^{(q)}, \quad (29)$$

where R_{kq} is unitary. Such a transformation induces new supermode nonlinear Lindblad operators of the form

$$\hat{L}_{\text{nl}}^{(k)} := \sum_q R_{kq} \hat{L}_{\text{nl}}^{(q)} = \sum_{m,n} \underbrace{R_{k,m+n} F_{mn}}_{F_{mn}^{(k)}} \hat{s}_m \hat{s}_n. \quad (30)$$

Whereas $\hat{L}_{\text{nl}}^{(q)}$ describes the coupling of the system to frequency modes of the reservoir at ω_{pq} , $\hat{L}_{\text{nl}}^{(k)}$ describes the coupling to reservoir supermodes in the pump band consisting of a superposition of different pump frequencies, with weights R_{kq} . Note that in the last equality, we assume a rotating wave approximation on (17)—as would

be appropriate for the SPOPOs considered in Sect. III—but the procedure is identical for the more general case.

At the same time, it is also possible to apply any arbitrary basis transformation on the signal modes, to define signal supermode operators

$$\hat{S}_i := \sum_m T_{im} \hat{s}_m, \quad (31)$$

where T_{im} is also unitary. This induces a corresponding transformation of the signal reservoir operators into supermode reservoir operators

$$\hat{B}_t^{(i)} := \sum_m T_{im} \hat{b}_t^{(m)}, \quad (32)$$

and hence also a transformation of the linear Lindblad operators into supermode ones:

$$\hat{L}'_{\text{lin}}{}^{(i)} := \sum_m T_{im} \hat{L}_{\text{lin}}^{(m)} = \sum_m T_{im} \sqrt{2\kappa_m} \hat{s}_m. \quad (33)$$

After performing these basis transformations, the supermode Lindblad operators can be furthermore written in terms of the signal supermodes as

$$\hat{L}'_{\text{lin}}{}^{(i)} = \sqrt{2} \sum_j \underbrace{\left(\sum_m \sqrt{\kappa_m} T_{im} T_{jm}^* \right)}_{K_{ij}} \hat{S}_j \quad (34a)$$

$$\hat{L}'_{\text{nl}}{}^{(k)} = \sum_{i,j} \underbrace{\left(\sum_{m,n} F_{mn}^{(k)} T_{im}^* T_{jn} \right)}_{G_{ij}^{(k)}} \hat{S}_i \hat{S}_j. \quad (34b)$$

The utility of this form is that, for physically realistic cases where $f_{mn}^{(q)}$ is relatively smooth (i.e., “low-rank”) in the mode indices—as depicted in Fig. 2, for example—the physics of the OPO is most concisely described using a supermode basis for both pump and signal. In such cases, we can single out one nonlinear Lindblad operator to pump, while at the same time identifying a single signal supermode as the dominant degree of freedom in the cavity. The consequence is that in (34), we need only consider a small range for the indices (i, j, k) to accurately describe the physics, allowing us to truncate the interaction matrix $G_{ij}^{(k)}$.

To make the above discussion more concrete, consider the SPOPO with nonlinear coefficients given by Fig. 2(c). Suppose we would like to pump this SPOPO using a Gaussian spectrum centered on $2\omega_0$, with N_p comb lines spanning from the center to where the power falls to $1/e$. Then a good choice for pump supermodes are the Hermite-Gaussian functions:

$$R_{kq} = \frac{1}{(\sqrt{\pi} N_p 2^k k!)^{1/2}} H_k(q/N_p) e^{-(q/N_p)^2/2}, \quad (35)$$

where H_k is the physicists’ Hermite polynomial of order k . This set of pump supermodes is illustrated in Fig. 3(a), and the resulting coefficients of the supermode nonlinear Lindblad operators are shown in Fig. 4(a).

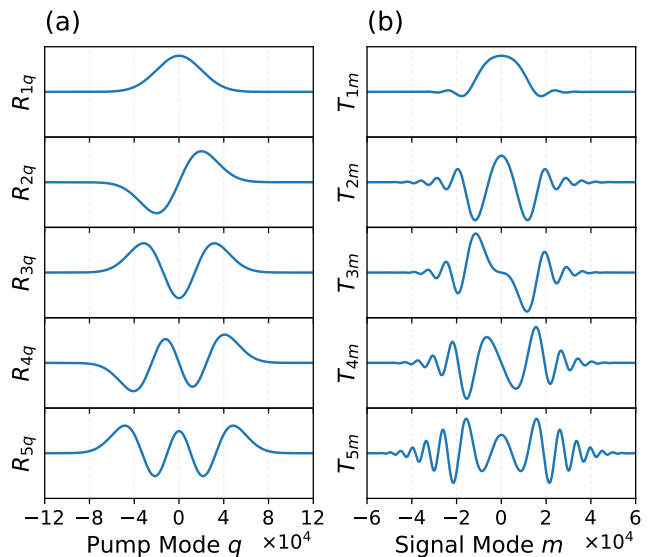


FIG. 3. Basis transformations on (a) pump reservoir modes and (b) signal cavity modes used to derive the simplified nonlinear Lindblads in Fig. 4, based on an SPOPO with dispersion parameters from Fig. 2(c). In (a), the pump supermode basis R_{kq} is chosen to be Hermite-Gaussian functions (35) with $N_p = 2 \times 10^4$, and in (b), the signal supermode basis T_{im} diagonalizes $G_{ij}^{(1)}$ in Fig. 4(b).

Next, we can choose the signal supermodes T_{im} such that the matrix $G_{ij}^{(1)}$, for example, is diagonal. This set of signal supermodes is shown in Fig. 3(b), and the resulting coefficients of the supermode nonlinear Lindblad operators written in terms of these signal supermodes are illustrated in Fig. 4(b). As we can see, $G_{ij}^{(1)}$ is indeed diagonal, with an eigenvalue spectrum dominated by only a few supermodes, due to the smoothness of the interactions. This results in a more economical description of the relevant nonlinear Lindblad operators on the system.

Diagonalizing $G_{ij}^{(1)}$ is especially convenient because if we pump the SPOPO with field strength \mathcal{A} using a pump spectrum $\alpha^{(q)} = \mathcal{A} R_{1q}$, we simply get

$$\hat{L}'_{\text{nl}}{}^{(1)} \mapsto \hat{L}'_{\text{nl}}{}^{(1)} + \mathcal{A}, \quad (36)$$

while all the other Lindblad operators remain invariant. Furthermore, the squeezing Hamiltonian (22) becomes

$$\hat{H}_{\text{sys}} = \frac{i\mathcal{A}}{2} \sum_i \Lambda_i \hat{S}_i^2 + \text{H.c.}, \quad (37)$$

where Λ_i is the i th eigenvalue of $G_{ij}^{(1)}$. This Hamiltonian describes a series of independent squeezing terms in the supermodes \hat{S}_i , in agreement with the physics obtained by Ref. [34] for an SPOPO below threshold after a supermode decomposition. By adding the nonlinear Lindblad operators written in the form (34b), that same economical description of the physics can be smoothly interpolated into the nonlinear above-threshold regime.

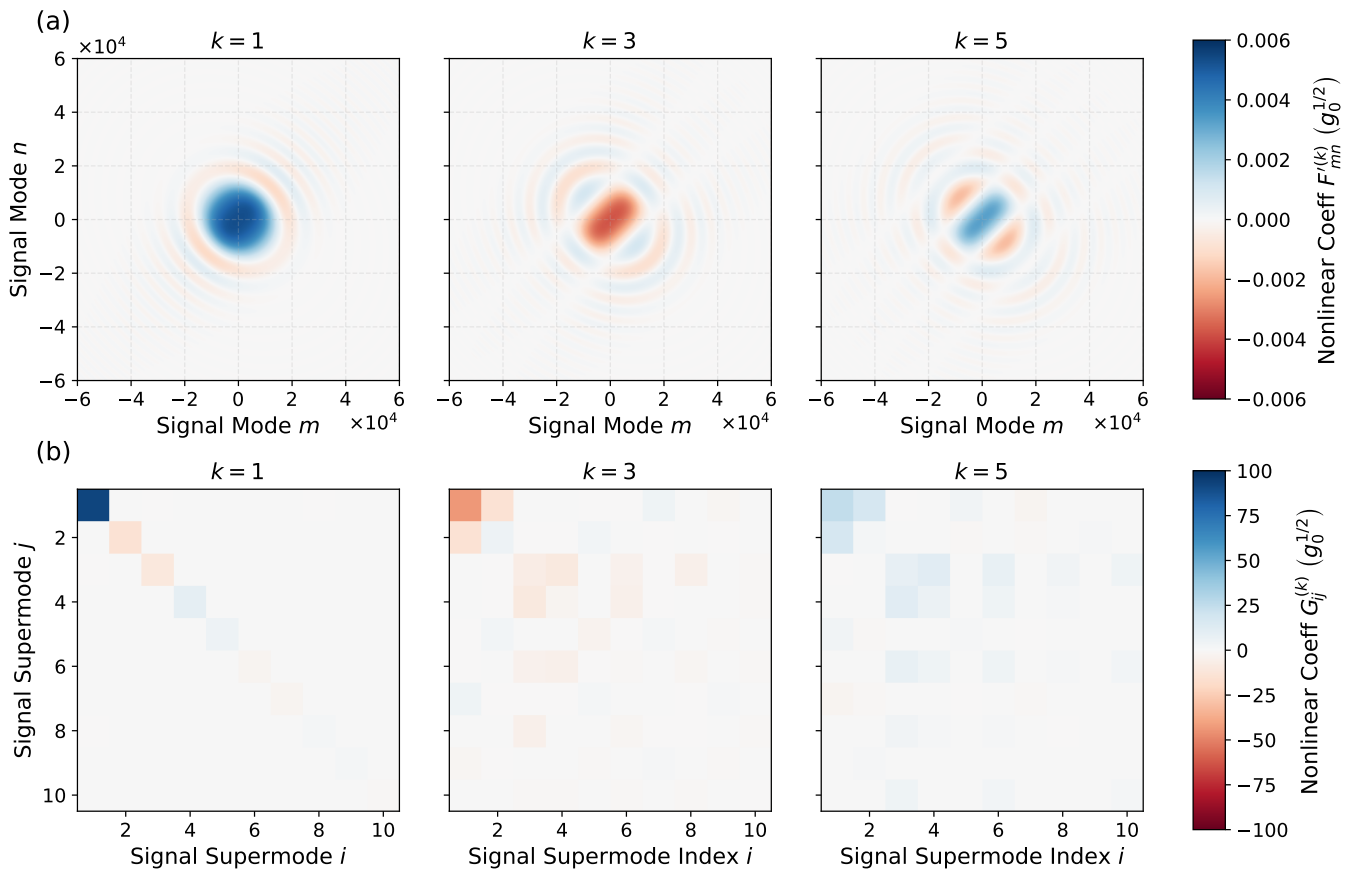


FIG. 4. Nonlinear coupling coefficients of the supermode nonlinear Lindblads $\hat{L}^{(k)}$, written in terms of (a) the signal frequency modes (i.e., $F_{mn}^{(k)}/\sqrt{g_0}$ from (30)), and (b) the signal supermodes (i.e., $G_{ij}^{(k)}/\sqrt{g_0}$ from (34b)). The system under consideration is the SPOPO with dispersion parameters from Fig. 2(c). Note that for even values of k , the supermode nonlinear Lindblads are identically zero and are not shown here. The corresponding supermode spectra are shown in Fig. 3.

VI. RESULTS

Having established the formalism of the model, it is useful to highlight and discuss in some detail how the model relates to known phenomenology of pulsed OPOs. We first revisit some of the assumptions made in the theory and identify their physical implications. Next, we look at the quantum Heisenberg equations of motion, which exhibit not only Gaussian effects like phase-sensitive amplification and squeezing, but also non-Gaussian physics like threshold and intensity-dependent loss. Third, we perform numerical simulations in the highly nonlinear regime that highlight the effects of quantum nonlinearity on multimode squeezing, signal/pump output spectra, and non-Gaussian state generation.

A. The white-noise approximation

The key simplifying assumption in this model is that the reservoir operators $\hat{b}_t^{(m)}$ and $\hat{a}_t^{(k)}$ have delta-function commutators in time and therefore act as independent

bosonic modes. In single-mode input-output theory, this white-noise assumption is afforded by the fact that the coupling between the system and the bath is constant over a bandwidth larger than the rates of any system interactions. That is, when defining the reservoir operators

$$\hat{b}_t^{(\text{cw})} := \int_{\mathcal{B}} \frac{d\omega}{2\pi} \hat{b}_\omega e^{-i\omega t}, \quad [\hat{b}_\omega^\dagger, \hat{b}_{\omega'}] = 2\pi\delta(\omega - \omega'), \quad (38)$$

the band \mathcal{B} is taken to have bandwidth greater than any system coupling rate (e.g., in the Hamiltonian or the linewidth). As a result, any excitations in these “time-bin” modes represented by $\hat{b}_t^{(\text{cw})}$ are very short compared to the time scale of the system dynamics, in which case we think of the interactions of these modes with the system to be independent, sequential events. Physically, the primary limitation to the bandwidth of \mathcal{B} in most cw systems is the free spectral range (FSR) of the cavity: for an FSR of, say, 100 MHz, numerical simulations produced by input-output theory are representative of the true physics down to the 10 ns scale, and it is rarely necessary to consider interactions occurring faster than this in cw systems.

Some subtleties arise when we consider a pulsed system; to be concrete, let us consider the SPOPO with repetition rate Ω . Once again, the bandwidth of \mathcal{S}_m used to define $\hat{b}_t^{(m)}$ in (3) must be on the order of Ω , or else we would run up against other cavity resonances an FSR away. Then, as long as the system interaction rates (e.g., $|\mathcal{A}|^2$, $G_{ij}^{(k)2}$ and κ_m) are small compared to Ω , it is possible to formulate an input-output theory based on the white-noise approximation, as described in Sect. II. Thus, the time index on $\hat{b}_t^{(m)}$ is analogous to the corresponding time index on the single-mode operators $\hat{b}_t^{(\text{cw})}$, while the mode index m simply labels a frequency multiplexing of the comb into the bands \mathcal{S}_m (and similarly for the pump).

In a pulsed system, however, it is also natural to think about the dynamics on a pulse-by-pulse basis. In this context, the fact that the bandwidths of the reservoir operators are limited to Ω means that this roundtrip-by-roundtrip picture cannot be faithfully captured by the theory once the white-noise approximation is made. For example, we know from physical intuition that in an SPOPO without scattering losses, the pulse amplitude should only reduce when the pulse envelope hits the out-coupler; at single-roundtrip time scales, this is effectively a *discrete* phenomenon. But if we instantiate a coherent state of the first supermode \hat{S}_1 in the cavity and zoom into its dynamics on sub-roundtrip-time scales, we see from the Heisenberg equations of motion (39) that the expectation value of the field decays *continuously* in time, contrary to physical intuition. However, provided $\kappa \ll \Omega$, the behavior of the system at longer time scales of multiple round trips (e.g., the ringdown envelope of

the pulses) is correctly reproduced. As this effect is a natural consequence of formulating an input-output theory for pulsed OPOs, it is also a prominent feature of the model described in Refs. [33, 34].

From this discussion, we see that results derived from making the white-noise approximation hold when the pulses do not experience dramatic changes over a single roundtrip or upon passing through a single optical element, a condition analogous to similar approximations made in classical pulsed nonlinear optics [41]. This approximation is a good characterization of pulsed OPOs with typical material nonlinearities and relatively low loss [42] such as those found in the experiments of Refs. [6, 10]. For high-gain, high-loss pulsed OPOs, however, it is possible input-output theory would need significant modifications or even outright replacement in favor of a free-field formulation, such as by quantizing nonlinear classical field equations modeling pulse propagation at sub-roundtrip time scales [43, 44].

B. SPOPO equations of motion

As alluded to in Sect. V, equations (20a) through (22) for the SPOPO can be recast in supermode form, using (34). Using standard input-output theory, we can derive the Heisenberg equations of motion describing the SPOPO quantum dynamics (formally, as a quantum stochastic differential equation in Itô form [21]). Assuming a coherent drive of amplitude $\mathcal{A}^{(k)}$ on each pump supermode R_{kq} , we have

$$\frac{d\hat{S}_i}{dt} = - \sum_j (K^\dagger K)_{ij} \hat{S}_j - \sum_{j,k} 2\mathcal{A}^{(k)} G_{ij}^{(k)} \hat{S}_j^\dagger - \sum_{j,m,n,k} G_{ij}^{(k)} G_{mn}^{(k)} \hat{S}_j^\dagger \hat{S}_m \hat{S}_n + \sum_j \sqrt{2} K_{ij} \hat{B}_t^{(j)} - \sum_{k,j} 2G_{ij}^{(k)} \hat{S}_j^\dagger \hat{A}_t^{(k)}, \quad (39)$$

along with the corresponding quantum input-output relations for the reservoir operators:

$$\hat{B}^{(i)} = \hat{B}^{(i)} + \sum_j \sqrt{2} K_{ij} \hat{S}_j \quad (40a)$$

$$\hat{A}^{(k)} = \hat{A}^{(k)} + \mathcal{A}^{(k)} + \sum_{ij} G_{ij}^{(k)} \hat{S}_i \hat{S}_j, \quad (40b)$$

where $\hat{B}^{(i)}$ and $\hat{A}^{(k)}$ ($\hat{B}^{(i)}$ and $\hat{A}^{(k)}$) are input (output) quantum white-noise operators for the signal and pump, respectively. These equations are in agreement with those derived by Ref. [34], following an appropriate transformation into the supermode basis.

The first term describes linear decay of the signal supermodes. When the reservoir coupling profile κ_m do not exactly match the chosen supermodes T_{im} , linear dissipation actually induces couplings between the different supermodes; this effect can potentially be useful for, e.g.,

designing couplings in coherent Ising machines [29]. A useful special case to consider is $\kappa_m = \kappa$, a constant for all m . Then $(K^\dagger K)_{ij} = \kappa \delta_{ij}$, so this term becomes $-\kappa \hat{S}_i$.

The second term is the OPO gain, responsible for the generation of signal excitation from pump driving, as well as phase-sensitive gain (phase-sensitive due to the dagger on \hat{S}_j^\dagger) and squeezing. In general, this squeezing is multimode, but per the discussion in Sect. V, we can choose to pump in the first supermode, so that $\mathcal{A}^{(1)} = \mathcal{A}$, a constant, with all others zero. If we furthermore assume that the signal supermode basis T_{im} was chosen to diagonalize $\hat{G}_{ij}^{(1)}$ with eigenvalues Λ_i , this term becomes $-2\mathcal{A} \Lambda_i \hat{S}_i^\dagger$.

The third term describes the nonlinear interaction among different signal supermodes resulting from a three-photon interaction with the reservoir at the pump. Formally, this term (along with its associated noise term) is discarded in a linear treatment of SPOPOs [34]. Intuitively, its role is to provide a nonlinear clamping mech-

anism to stabilize the system when the gain produced by the second term exceeds the linear loss induced by the first term, resulting in a finite threshold; this can be seen most readily in the single-supermode case where this term $\propto -(\hat{S}^\dagger \hat{S}) \hat{S}$, signifying an intensity-dependent field decay. In general, this term is both multimode and nonlinear: any residual structure in the coupling factors $G_{ij}^{(k)} G_{mn}^{(k)}$ not captured by the supermode diagonalization show up here and produces nonlinear couplings among the supermodes that experience gain.

The fourth and fifth terms are quantum noise terms that describe the interaction between the signal supermodes and the reservoir, the first at the signal frequency band due to linear dissipation, and the second at the pump frequency band due to nonlinear parametric interactions. As before, the linear dissipation can induce couplings between different supermodes if κ_m is arbitrary; for the special case of constant $\kappa_m = \kappa$, this term also becomes uncoupled and reads $\sqrt{2\kappa} \hat{B}_i^{(i)}$.

The input-output relations (40a) and (40b) also provide some insight into the physics of the SPOPO. In (40a), we again see a mode-mixing term due to linear outcoupling/scattering; in the special case where $K_{ij} = \sqrt{\kappa} \delta_{ij}$, this just reads $\sqrt{2\kappa} \hat{S}_j$. Equation (40b) is more interesting, as the nonlinear interaction with the cavity produces a two-photon contribution to the outgoing field, which can be thought of as resonant, broadband second-harmonic generation, or, alternatively, a model for back-conversion of signal light back into pump light. This is a multimode effect, as the spectral profile of the nonlinear interaction need not be (and in general cannot be) fully matched to our choice of the signal supermodes. Furthermore, when the sign of the back-conversion (i.e., the sign of $\sum_{ij} G_{ij}^{(k)} \hat{S}_i \hat{S}_j$) becomes out of phase with the drive amplitude $\mathcal{A}^{(k)}$, interference between the back-converted light and the input pump light manifests as pump depletion. In a linearized theory consistent with discarding the nonlinear terms of (39), the latter term in (40b) is also omitted.

C. Numerical simulations

To perform numerical simulations, it is helpful to make various simplifying assumptions as mentioned throughout this paper. We consider an SPOPO as described in Sect. III, with nonlinear interactions governed by the phase-matching assumptions made in Sect. IV; specifically, we consider the dispersion parameters as shown in Fig. 2(c). Following Sect. V, we recast the physics in supermode form, by pumping with strength \mathcal{A} in the first Hermite-Gaussian pump supermode R_{1q} as in (35) and choosing the signal supermodes T_{im} to diagonalize the interactions $G_{mn}^{(1)}$, with resulting eigenvalues Λ_i , corresponding to the eigenvectors T_{im} ; these transformations correspond to those shown in Fig. 4. Finally, we assume that $\kappa_m \approx \kappa$ a constant, as discussed in Sect. VI B.

Explicitly, we choose for our Hamiltonian and Lindblad operators the following model:

$$\frac{\hat{H}_{\text{sys}}}{\kappa} = \frac{ir}{4} \sum_i \frac{\Lambda_i}{\Lambda_1} \hat{S}_i^2 + \text{H.c.} \quad (41a)$$

$$\frac{\hat{L}'_{\text{lin}}}{\sqrt{\kappa}} = \sqrt{2} \hat{S}_i \quad (41b)$$

$$\frac{\hat{L}'_{\text{nl}}}{\sqrt{\kappa}} = \sqrt{\eta} \sum_{ij} \frac{G_{ij}^{(k)}}{\Lambda_1} \hat{S}_i \hat{S}_j + \frac{r}{2\sqrt{\eta}} \delta_{k1}, \quad (41c)$$

where $\Lambda_i = G_{ii}^{(1)}$ after diagonalization and we have introduced dimensionless parameters

$$r := \frac{2\mathcal{A}\Lambda_1}{\kappa} \quad \text{and} \quad \eta := \frac{\Lambda_1^2}{\kappa}. \quad (42)$$

The parameter r is the pump parameter, representing (in the mean-field) the number of times the pump strength lies above the threshold of the first supermode, in units of field (i.e., r^2 is the pump parameter in power). The parameter η is the ratio between the intensity-dependent and the linear decay rates of the first supermode (i.e., the rate of the third term in (39) at $i = j = k = m = n = 1$). These dimensionless parameters incorporate the pump strength \mathcal{A} and the scale g_0 of the nonlinear coupling coefficients. More specifically, we set $1/\kappa$ as the unit of time, and for a given η , we fix g_0 in Fig. 4(b) such that $\Lambda_1 = \sqrt{\kappa\eta}$, while for a given r , we fix $\mathcal{A} = \kappa r / 2\Lambda_1$.

We perform numerical simulations in Julia using the QuantumOptics.jl package [45]. We simulate state evolution equations in standard quantum input-output theory, which we summarize in Appendix for convenience. We take advantage of the supermode decomposition to truncate the multimode simulation to a small number of signal modes—four in Fig. 5 (i.e., $1 \leq i \leq 4$) and five in Fig. 6 and 7 (i.e., $1 \leq i \leq 5$)—as well as to the first forty nonlinear Lindblad operators (i.e., $1 \leq k \leq 40$), discarding even values of k as noted in Fig. 4. To check that our choices for numerical truncation are appropriate, we repeat calculations with increasing thresholds for truncation until we arrive at results that do not qualitatively change upon increase.

Fig. 5(a) shows the steady-state squeezing spectrum $S_{\text{hom}}(\omega)$ of the first signal supermode \hat{S}_1 , computed as a function of pump parameter in the highly nonlinear regime of $\eta = 1$. For comparison, we also show in Fig. 5(b) the analytic squeezing spectrum

$$S_{\text{hom}}^{(\text{lin})}(\omega) = \frac{\omega^2 + \kappa^2(1+r)^2}{\omega^2 + \kappa^2(1-r)^2}, \quad (43)$$

obtained by linearizing the equations of motion (39) as done in Ref. [34] (corresponding to $\eta \rightarrow 0$). As we can see, the nonlinear model allows us to calculate squeezing beyond the threshold point of $r = 1$ where the linearized model breaks down. In addition, the spectra are markedly different in appearance: in the regime of

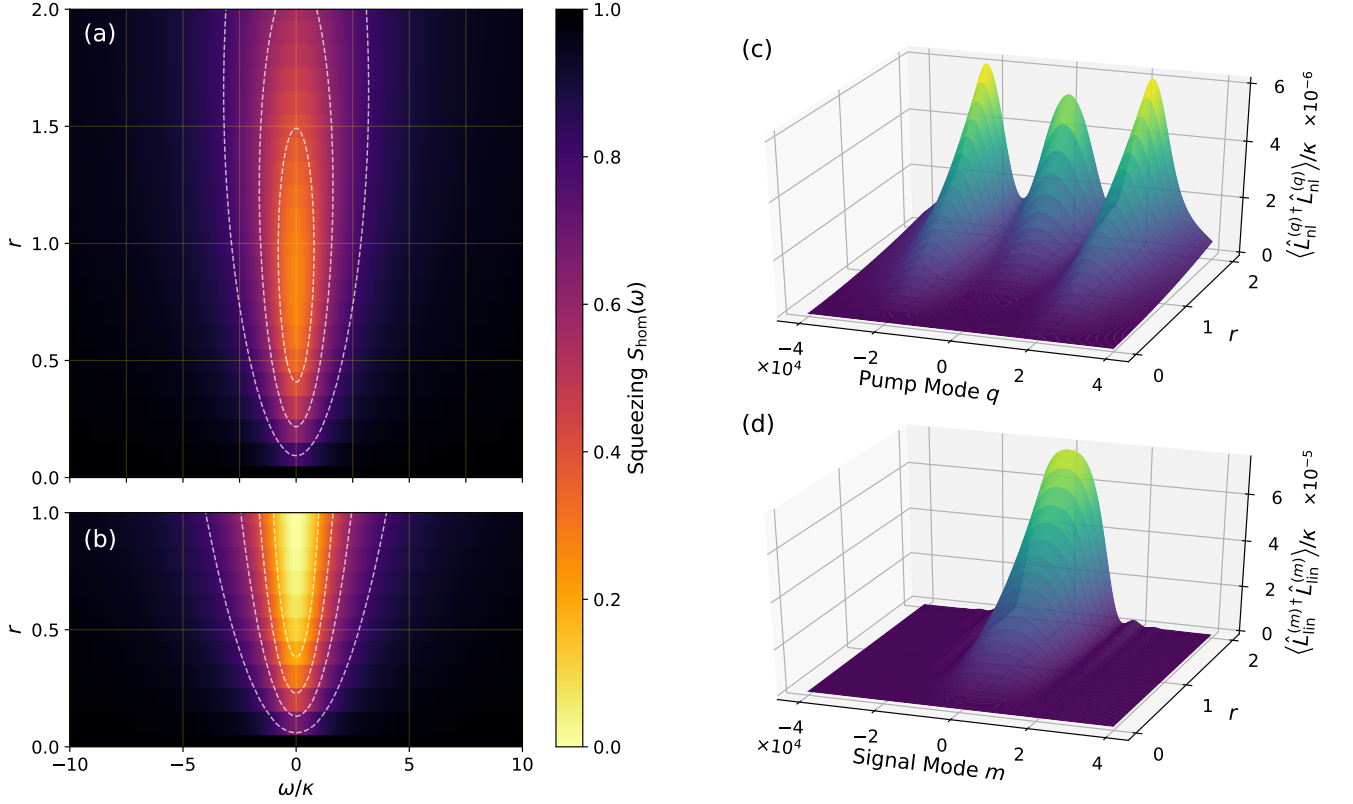


FIG. 5. Numerical simulation results for an SPOPO with nonlinear coefficients from Fig. 4(b). (a,b) Steady-state squeezing spectrum $S_{\text{hom}}(\omega)$ (vacuum level normalized to one) of the first signal supermode as a function of pump parameter r using (a) the nonlinear model in (41) with $\eta = 1$, and (b) the analytic linearized model of (43). (c,d) Steady-state output photon flux spectrum of (c) the pump, given by $\langle \hat{L}_{\text{nl}}^{(q)\dagger} \hat{L}_{\text{nl}}^{(q)} \rangle / \kappa$, and (d) the signal, given by $\langle \hat{L}_{\text{lin}}^{(m)\dagger} \hat{L}_{\text{lin}}^{(m)} \rangle / \kappa$, as functions of pump parameter r using the nonlinear model in (41) with $\eta = 1$.

high nonlinearity, both the bandwidth and the degree of squeezing are limited, which is in accordance with the results of Ref. [46]. These results are consistent with the fact that, at $\eta/\kappa \sim 1$, threshold as a mean-field concept is no longer sharply defined, as the mean photon number in the vacuum squeezed state “below threshold” ($r < 1$) is comparable to the mean photon number in the bright state “above threshold” ($r > 1$).

In Fig. 5(c,d), we show steady-state optical spectra of the pump and signal outputs, also in the highly nonlinear regime of $\eta = 1$. Here, the spectrum is defined as (a) $\langle \hat{L}_{\text{nl}}^{(q)\dagger} \hat{L}_{\text{nl}}^{(q)} \rangle$ as a function of q and (b) $\langle \hat{L}_{\text{lin}}^{(m)\dagger} \hat{L}_{\text{lin}}^{(m)} \rangle$ as a function of m . These expectation values represent, for each frequency mode indexed by m or q , the mean photon flux emitted by the system at that frequency; these quantities constitute what one might measure, for example, on an optical spectrum analyzer. In the absence of any interaction with the SPOPO, the pump output spectrum follows the input pump spectrum, i.e., a Gaussian with amplitude dictated by r . As r is increased from zero, however, the pump spectrum in Fig. 5(c) exhibits pump depletion, represented by the diminished amplitude near the center of the spectrum where the interac-

tions are most closely phase-matched. This occurs even for $r < 1$, which is expected in this nonlinear regime where the threshold pump flux (i.e., $|\mathcal{A}|^2$ at $r = 1$) is comparable to κ . The pump depletion also correlates as expected with the intensity of the signal spectrum shown in Fig. 5(d). Further above threshold, this pump-depleted spectral region starts to fill up again, due to back-conversion of signal light into pump light, forming the central lobe seen in the plot at higher values of r .

To better understand the effects of the multimode nonlinear Lindblad in and of themselves, we also simulate the system in the absence of linear loss. This model can be obtained by a reparametrization of (41): we resubstitute η and r and cancel out κ in favor of parameterizing time in $1/\Lambda_1^2$. More specifically, we use the model

$$\frac{\hat{H}_{\text{sys}}}{\Lambda_1^2} = \frac{ip}{4} \sum_i \frac{\Lambda_i}{\Lambda_1} \hat{S}_i^2 + \text{H.c.} \quad (44a)$$

$$\frac{\hat{L}_{\text{nl}}^{(k)}}{\Lambda_1} = \sum_{ij} \frac{G_{ij}^{(k)}}{\Lambda_1} \hat{S}_i \hat{S}_j + \frac{p}{2} \delta_{k1}, \quad (44b)$$

where we define a new pump parameter $p := 2\mathcal{A}/\Lambda_1$.

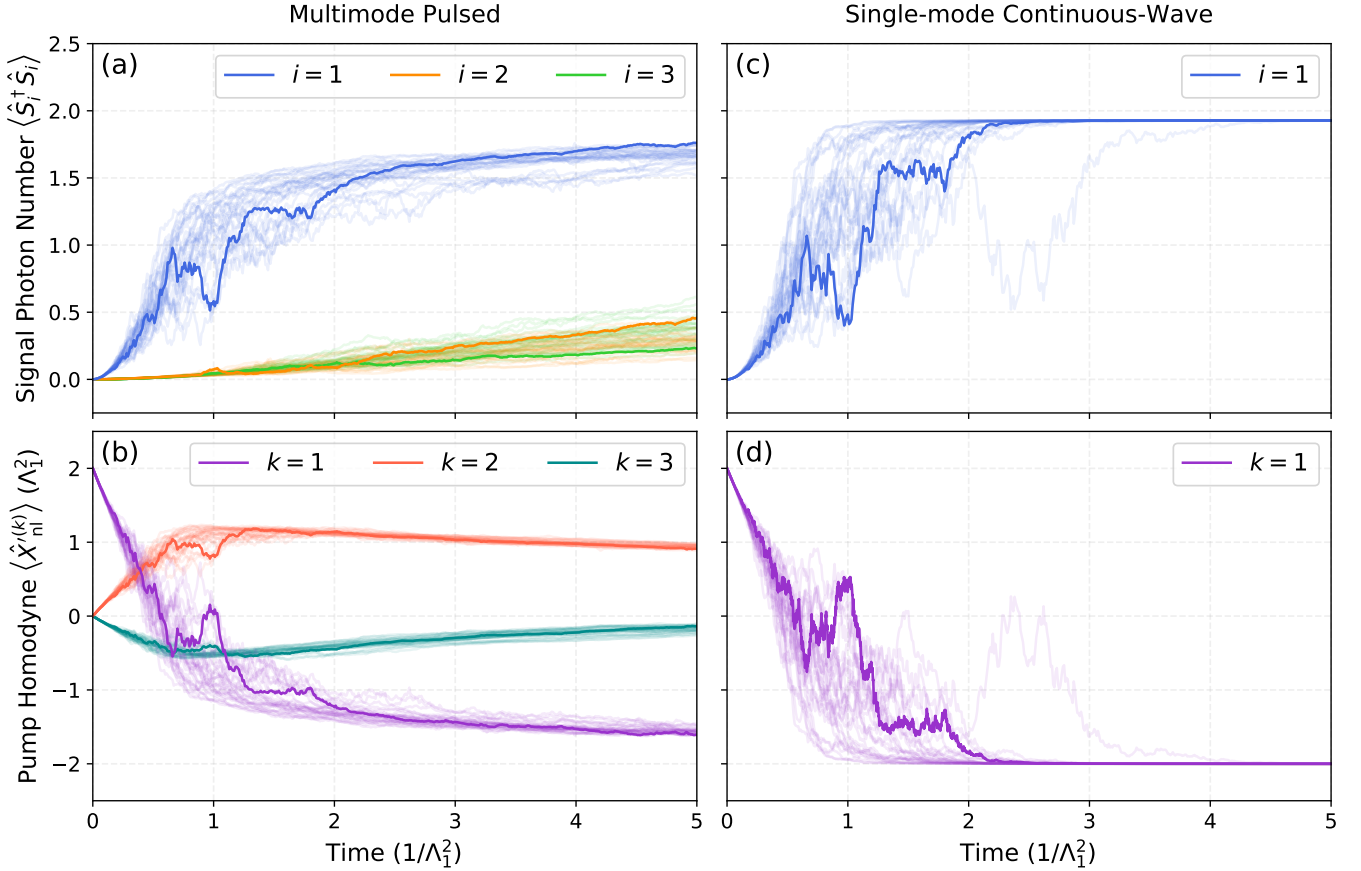


FIG. 6. Quantum trajectory simulations of (a,c) internal signal photon number and (b,d) mean in-phase pump homodyne current, under continuous monitoring of the nonlinear Lindblad operator(s) for two OPO models: in (a,b), a multimode SPOPO with nonlinear coefficients from Fig. 4(b) using the model in (44); and in (c,d), the corresponding single-mode cw OPO. In both cases, no linear loss is considered, and the pump parameter is set to $p = 2$. For comparison between the two models, the bolded trajectories indicate respective trajectories based on the same random number generator seed.

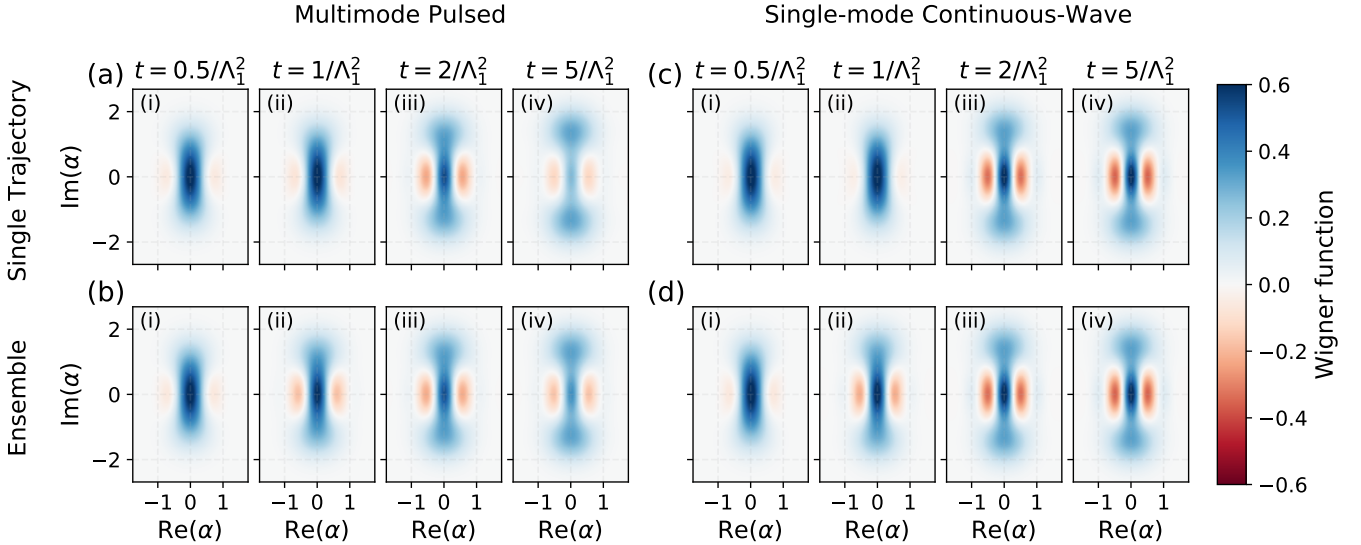


FIG. 7. Wigner functions of the first signal supermode for the two OPO models (multimode and single-mode) considered in Fig. 6, sampled at various points in time (indexed with lower-case roman numerals). In (a) and (c), we show the Wigner functions for the stochastic trajectories bolded in Fig. 6(a) and (c), respectively. In (b,d), we show the Wigner functions of the ensemble average over all trajectories for each model, computed via the unconditional master equation.

We are especially interested in comparing this multimode model to its corresponding single-mode cw version, which we define by restricting the indices appearing in (44) to $i = j = k = 1$ (i.e., neglecting all higher-order pump and signal supermodes). The phenomenology of such cw OPOs is well known; as shown in [14], the steady state in the absence of linear loss is the pure cat state $|i\sqrt{p}\rangle + |-i\sqrt{p}\rangle$ (i.e., a superposition of coherent states).

Fig. 6 shows quantum trajectories from solving the stochastic Schrödinger equation for an SPOPO and its corresponding cw OPO, at a pump parameter $p = 2$. As the only relevant Lindblad operators are the nonlinear ones, our choice of unraveling corresponds to an in-phase homodyne monitoring of the *pump* channels. The resulting trajectories provide direct evidence that multimode physics occurs in the SPOPO, as the signal photon numbers in higher-order supermodes ($i > 1$) grow with time, while nonzero homodyne signals are observed in higher-order pump supermodes ($k > 1$). In the initial transient period ($t < 2/\Lambda_1^2$), the trajectories for the multimode SPOPO show qualitatively similar stochastic variations to those for the single-mode cw OPO (e.g. in the mean and variance of their respective ensembles). Both OPOs also qualitatively respond in similar fashion to a single instantiation of quantum noise, as is evident from the bolded trajectories. After the transient period, however, the cw OPO quickly approaches steady state, whereas the SPOPO continues to evolve (specifically, the mean of the ensemble continues to change) due to still-increasing excitations in the higher-order supermodes. Finally, the SPOPO continues to exhibit fluctuations about the ensemble mean at later times, an effect which can be interpreted as decoherence since these fluctuations act to decrease the purity of the ensemble. Such residual fluctuations are absent in the cw OPO, consistent with the observation that a pure cat state is eventually formed in the single-mode case.

Similar conclusions can be reached by examining Fig. 7, which shows Wigner functions of the first supermode at various points in time, for both the bolded trajectories of Fig. 6 and for the respective ensemble averages (calculated from the unconditional master equation). As in Fig. 6, we observe that the Wigner functions of the SPOPO and cw OPO are qualitatively similar during the initial transient period (i.e., $t = 0.5/\Lambda_1^2, 1.0/\Lambda_1^2$). After this initial transient, the cw OPO quickly converges to its steady-state Wigner function, and the single trajectory looks similar to the ensemble average. On the other hand, the SPOPO on the single trajectory differs qualitatively from that of the ensemble average, indicating the presence of stochastic variations at later times. Interestingly, we also observe that at later times in the single trajectory of the SPOPO—for example, in Fig. 7(a)(iv)—the reduced state of the first supermode is impure despite the fact that the system state remains pure under conditional evolution. This indicates that the multimode interactions in an SPOPO also entangles the various signal supermodes when conditioning on pump homodyne.

VII. CONCLUSIONS

In this work, we investigated the modeling of nonlinear effects in ultrashort-pulse OPOs from the perspective of quantum input-output theory. By extending the supermode technique of Refs. [33, 34], we obtained a reduced description of the pump-signal interactions using a nonlinear Lindblad operator formalism. In the highly nonlinear regime, we observed by numerical simulation nonlinear effects such as pump depletion and back-conversion of signal to pump. We found that, as expected, non-Gaussian physics in this regime can produce intracavity states with Wigner function negativity, but at the same time, multimode interactions can play a nontrivial role in their dynamics and dissipation.

From a technological perspective, the large enhancements of the nonlinear coupling rate in ultrashort-pulse OPOs (in the form of the supermode eigenvalue Λ_1) can potentially open a path towards quantum-scale nonlinearities in an all-optical platform. In this context, the multimode interactions present interesting challenges to the problem of quantum state generation, and we suspect that the decoherence into the reservoir via pump supermodes can be mitigated by appropriate engineering of the multimode interactions; the result of numerical investigations to this end will be reported in a future publication.

In the meantime, quantum simulations in the intermediate (i.e., moderately nonlinear) regime are also important to the characterization of near-term pulsed OPOs, but unlike in the highly nonlinear regime we considered here, such simulations can be numerically challenging due to large signal excitations. However, for quantum input-output models, there have been recent developments in numerically reparameterizing open quantum system dynamics using, for example, manifold techniques based on coherent displacements and squeezing operations [47]. A multimode implementation of such numerical schemes can potentially be applied to study pulsed OPOs in this intermediate regime.

ACKNOWLEDGMENTS

The authors wish to thank R. Yanagimoto, D. G. Gray, and L. G. Wright for helpful discussions.

T. O., E. N., and H. M. acknowledge funding from NSF award PHY-1648807. R.H. is supported by an IC Postdoctoral Research Fellowship at MIT, administered by ORISE through U.S. DOE and ODNI. N.L. acknowledges funding from the Swiss SNSF. P.L.M. acknowledges support from the Impulsing Paradigm Change through Disruptive Technologies (ImPACT) Program of the Council of Science, Technology and Innovation (Cabinet Office, Government of Japan) and also a Stanford Nano- and Quantum Science and Engineering Postdoctoral Fellowship. A.M. acknowledges funding from ARO award W911NF-18-1-0285.

Appendix: Simulation method

In this section, we briefly review the key results from input-output theory we utilize in the numerical simulations of Sect. VIC. Most of the formulas in this section follow the presentation in Ref. [18].

We obtain the unconditional evolution of the system density matrix $\rho(t)$ using the master equation in Lindblad form [48]:

$$\frac{d\hat{\rho}}{dt} = -i[\hat{H}_{\text{sys}}, \hat{\rho}] + \sum_i \hat{L}_i \hat{\rho} \hat{L}_i^\dagger - \frac{1}{2} \sum_i \{\hat{L}_i^\dagger \hat{L}_i, \hat{\rho}\}, \quad (\text{A.1})$$

where \hat{H}_{sys} is the system Hamiltonian and \hat{L}_i enumerate all the Lindblad operators of the system.

To compute the steady-state density matrix $\hat{\rho}_{\text{ss}}$ satisfying $d\hat{\rho}_{\text{ss}}/dt = 0$, we simulate (A.1) to a sufficiently large time T such that $\hat{\rho}(t > T) \approx \hat{\rho}(T)$.

To obtain the steady-state squeezing spectrum that results from performing homodyne detection on a port represented by a particular Lindblad operator \hat{L} (e.g., $\hat{L} = \sqrt{2\kappa}\hat{S}_1$), we first compute the steady-state homodyne correlation function

$$F_{\text{hom}}(\tau) = \text{tr} \left[(\hat{L} + \hat{L}^\dagger) \hat{A}(\tau) \right] + \delta(\tau), \quad (\text{A.2})$$

where $A(\tau)$ is the solution to the differential equation

$$\frac{d\hat{A}}{d\tau} = -i[\hat{H}_{\text{sys}}, \hat{A}] + \sum_i \hat{L}_i \hat{A} \hat{L}_i^\dagger - \frac{1}{2} \sum_i \{\hat{L}_i^\dagger \hat{L}_i, \hat{A}\} \quad (\text{A.3})$$

with initial condition $\hat{A}(0) = \hat{L}\hat{\rho}_{\text{ss}} + \hat{\rho}_{\text{ss}}\hat{L}^\dagger$. The squeezing spectrum is then the Fourier transform of the correlation function:

$$S_{\text{hom}}(\omega) := \int_{-\infty}^{\infty} e^{-i\omega\tau} F_{\text{hom}}(\tau) d\tau. \quad (\text{A.4})$$

To obtain conditional evolution, we simulate the stochastic Schrödinger equation (SSE), by solving the unnormalized SSE numerically and normalizing the state at every timestep. The unnormalized SSE is

$$d|\bar{\psi}\rangle = \left(\hat{f} dt + \sum_i \hat{g}_i dW_i \right) |\bar{\psi}\rangle, \quad (\text{A.5})$$

where dW_i are differentials of independent standard Weiner processes, and the deterministic and stochastic components of the stochastic differential equation are, respectively,

$$\hat{f} := -i\hat{H}_{\text{sys}} + \sum_i \left(-\frac{1}{2} \hat{L}_i^\dagger \hat{L}_i + \langle \hat{L}_i + \hat{L}_i^\dagger \rangle \hat{L}_i \right) \quad (\text{A.6})$$

$$\hat{g}_i := \hat{L}_i. \quad (\text{A.7})$$

-
- [1] F. Adler, K. C. Cossel, M. J. Thorpe, I. Hartl, M. E. Fermann, and J. Ye, *Opt. Lett.* **34**, 1330 (2009).
 - [2] T. J. Kippenberg, R. Holzwarth, and S. A. Diddams, *Science* **332**, 555 (2011).
 - [3] B. Spaun, P. B. Changala, D. Patterson, B. J. Bjork, O. H. Heckl, J. M. Doyle, and J. Ye, *Nature* **533**, 517 (2016).
 - [4] A. Marandi, K. A. Ingold, M. Jankowski, and R. L. Byer, *Optica* **3**, 324 (2016).
 - [5] R. W. Boyd, *Nonlinear Optics* (Academic Press, 2008) p. 613.
 - [6] J. Roslund, R. M. De Araujo, S. Jiang, C. Fabre, and N. Treps, *Nat. Photonics* **8**, 109 (2014).
 - [7] S. Gerke, J. Sperling, W. Vogel, Y. Cai, J. Roslund, N. Treps, and C. Fabre, *Phys. Rev. Lett.* **114**, 050501 (2015).
 - [8] R. M. Shelby and M. Rosenbluh, *Appl. Phys. B Photo-physics Laser Chem.* **55**, 226 (1992).
 - [9] N. C. Menicucci, P. van Loock, M. Gu, C. Weedbrook, T. C. Ralph, and M. A. Nielsen, *Phys. Rev. Lett.* **97**, 110501 (2006).
 - [10] G. Ferrini, J. Roslund, F. Arzani, Y. Cai, C. Fabre, and N. Treps, *Phys. Rev. A* **91**, 032314 (2015).
 - [11] Y. Cai, J. Roslund, G. Ferrini, F. Arzani, X. Xu, C. Fabre, and N. Treps, *Nat. Commun.* **8**, 1 (2017).
 - [12] B. Brecht, D. V. Reddy, C. Silberhorn, and M. Raymer, *Phys. Rev. X* **5**, 041017 (2015).
 - [13] L.-A. Wu, M. Xiao, and H. J. Kimble, *J. Opt. Soc. Am. B* **4**, 1465 (1987).
 - [14] M. D. Reid and L. Krippner, *Phys. Rev. A* **47**, 552 (1993).
 - [15] S. L. Braunstein and P. van Loock, *Rev. Mod. Phys.* **77**, 513 (2005).
 - [16] T. Gehring, V. Händchen, J. Duhme, F. Furrer, T. Franz, C. Pacher, R. F. Werner, and R. Schnabel, *Nat. Commun.* **6**, 8795 (2015).
 - [17] C. Gardiner and M. Collett, *Phys. Rev. A* **31**, 3761 (1985).
 - [18] H. Wiseman and G. Milburn, *Quantum Measurement and Control* (Cambridge University Press, 2010).
 - [19] C. W. Gardiner, A. S. Parkins, and P. Zoller, *Phys. Rev. A* **46**, 4363 (1992).
 - [20] H. M. Wiseman and G. J. Milburn, *Phys. Rev. A* **47** (1993).
 - [21] J. Combes, J. Kerckhoff, and M. Sarovar, *Adv. Phys. X* **2**, 784 (2017).
 - [22] H. J. Carmichael, *Phys. Rev. Lett.* **70**, 2273 (1993).
 - [23] O. Crisafulli, N. Tezak, D. B. S. Soh, M. A. Armen, and H. Mabuchi, *Opt. Express* **21**, 18371 (2013).
 - [24] S. Iida, M. Yukawa, H. Yonezawa, N. Yamamoto, and A. Furusawa, *IEEE Trans. Automat. Contr.* **57**, 2045 (2012).
 - [25] P. L. McMahon, A. Marandi, Y. Haribara, R. Hamerly, C. Langrock, S. Tamate, T. Inagaki, H. Takesue, S. Utsunomiya, K. Aihara, R. L. Byer, M. M. Fejer,

- H. Mabuchi, and Y. Yamamoto, *Science* **354**, 614 (2016).
- [26] A. Marandi, Z. Wang, K. Takata, R. L. Byer, and Y. Yamamoto, *Nat. Photonics* **8**, 937 (2014).
- [27] K. Takata, A. Marandi, and Y. Yamamoto, *Phys. Rev. A* **92**, 043821 (2015).
- [28] A. Yamamura, K. Aihara, and Y. Yamamoto, *Phys. Rev. A* **96**, 053834 (2017).
- [29] Z. Wang, A. Marandi, K. Wen, R. L. Byer, and Y. Yamamoto, *Phys. Rev. A* **88**, 18 (2013).
- [30] M. Mirrahimi, Z. Leghtas, V. V. Albert, S. Touzard, R. J. Schoelkopf, L. Jiang, and M. H. Devoret, *New J. Phys.* **16**, 045014 (2014).
- [31] A. Gilchrist, K. Nemoto, W. J. Munro, T. C. Ralph, S. Glancy, S. L. Braunstein, and G. J. Milburn, *J. Opt. B Quantum Semiclassical Opt.* **6**, S828 (2004).
- [32] W. J. Munro, K. Nemoto, G. J. Milburn, and S. L. Braunstein, *Phys. Rev. A* **66**, 023819 (2002).
- [33] G. J. de Valcárcel, G. Patera, N. Treps, and C. Fabre, *Phys. Rev. A* **74**, 061801 (2006).
- [34] G. Patera, N. Treps, C. Fabre, and G. J. de Valcárcel, *Eur. Phys. J. D* **56**, 123 (2010).
- [35] W. Wasilewski, A. I. Lvovsky, K. Banaszek, and C. Radzewicz, *Phys. Rev. A - At. Mol. Opt. Phys.* **73** (2006), 10.1103/PhysRevA.73.063819, 0512215.
- [36] P. Drummond and M. Hillery, *The Quantum Theory of Nonlinear Optics* (Cambridge University Press, 2014).
- [37] N. Quesada and J. Sipe, *Optics Letters* **42**, 3443 (2017).
- [38] Y. Yamamoto and A. Imamoglu, *Mesoscopic Quantum Optics* (John Wiley and Sons, 1999).
- [39] To obtain the case of type-I phase matching instead, take $\sqrt{g_{mn}} \rightarrow 2\sqrt{g_{mn}}, k_{\text{qpm}} \rightarrow 0$.
- [40] Here, as throughout the paper, $\text{sinc } x := \sin x/x$.
- [41] H. Haus, *IEEE J. Sel. Top. Quantum Electron.* **6**, 1173 (2000).
- [42] It is worth noting that these conditions do not conflict with our numerical study of SPOPOs in the “highly nonlinear” regime, which merely involves the *relative* scale the nonlinear coupling rate to the linear dissipation rate.
- [43] R. Hamerly, A. Marandi, M. Jankowski, M. M. Fejer, Y. Yamamoto, and H. Mabuchi, *Phys. Rev. A* **94**, 1 (2016).
- [44] M. Jankowski, A. Marandi, C. R. Phillips, R. Hamerly, K. A. Ingold, R. L. Byer, and M. M. Fejer, *Phys. Rev. Lett.* **120**, 053904 (2018).
- [45] S. Krämer, D. Plankensteiner, L. Ostermann, and H. Ritsch, *Computer Physics Communications* **227**, 109 (2018).
- [46] S. Chaturvedi, K. Dechoum, and P. D. Drummond, *Phys. Rev. A* **65**, 033805 (2002).
- [47] N. Tezak, N. H. Amini, and H. Mabuchi, *Phys. Rev. A* **96**, 062113 (2017).
- [48] The anticommutator is $\{\hat{A}, \hat{B}\} := \hat{A}\hat{B} + \hat{B}\hat{A}$.